Zn-Al layered double hydroxides as efficient photocatalysts for NOx abatement

Fredy Rodriguez-Rivas[1], Adrián Pastor, Cristobalina Barriga, Manuel Cruz-Yusta, Luis Sánchez* and Ivana Pavlovic*

Departamento de Química Inorgánica, Instituto Universitario de Investigación en Química Fina y Nanoquímica IUIQFN, Universidad de Córdoba, Campus de Rabanales, E-14071 Córdoba, España.

[1] Permanent Address : Departamento de Química. Facultad de Química y Farmacia. Universidad Nacional Autónoma de Tegucigalpa, Honduras.

* Corresponding Authors:

- Prof. Ivana Pavlovic

  ORCID ID: 0000-0003-2165-2940

  E-mail: pauli@uco.es

  Tel: +00-34-957-218648

- Prof. Luis Sánchez

  ORCID ID: 0000-0002-0194-1908

  E-mail: luis-sanchez@uco.es

  Tel: +00-34-957-218634

Abstract

In this study, we report that layered double hydroxides (LDH) exhibited high photocatalytic activities in degrading NOx gases for the first time. ZnAl-CO_3 LDHs with a 1.5 to 3.0 Zn/Al ratio were prepared by a coprecipitation method both with and without hydrothermal treatment. Syntheses were carried out with high and low metal concentrations, the latter being the most favorable in obtaining pure LDHs in the whole Zn/Al ratio range. The samples were characterized by different techniques such as PXRD, FT-IR, ICP mass, TGA, SBET, SEM and Diffuse reflectance (DR). The LDH particles grew as well-defined hexagonal nanolayers, whose size and crystallization depended on the synthetic procedure and the Zn/Al ratio. Those samples with lower crystallinity exhibit the highest specific surface area values (> 50 $m^2 \cdot g^{-1}$). The ZnAl-CO_3 LDHs were UV light responsive with band–gap values close to 3.5 eV. The LDH photocatalysts show a high performance towards the photochemical oxidation process of NO gas, with efficiencies of around 55 %. Remarkably, the ZnAl-CO_3 photocatalysts exhibit an impressive selectivity towards the deNOx process, avoiding the emission of the toxic NO_2 gas into the atmosphere. Interestingly, these promising deNOx results are repeated when working for a long irradiation period or with the highest concentration of NO in polluted atmospheres.

Keywords

LDH, Hydrotalcite, Photocatalyst, Nitrogen oxides

Highlights

- Zn-Al LDHs act as enhanced photocatalysts in deNO_X processes
- High NO conversion value for Zn-Al LDHs is obtained
- deNOx selectivity of LDH is superior to that of benchmark TiO_2
- Surface area of LDH samples affects NOx conversion more than their Zn/Al ratio

1. Introduction

The elimination of the gaseous pollutants is an environmental issue of huge scientific and social interest. Nitric oxide (NO) and nitrogen dioxide (NO_2) are together referred to as nitrogen oxide gases (NO_X) [1].The contamination of urban areas by NOx is becoming a severe environmental and human health issue, since many towns worldwide frequently suffer peaks in NOx contamination, far superior to the current legislation's approved values. Human health could be affected in several ways when NOx levels are high, as they cause diseases such as bronchitis, emphysema, cancer, etc. [2-4]. In fact, thousands of early deaths worldwide are associated with these NO_X emissions (72.000 in Europe in 2015).

Photocatalysis is one of the technologies that could be applied in the remediation of this problem, where TiO_2 and TiO_2-based compounds are more extensively studied as one of the most efficient photocatalytic systems for the oxidative decomposition of NOx (deNOx) [5-7]. In this sense, a broad catalogue of titania based photocatalytic building materials (benchmark products) is known today. However, in spite of its excellent performance as a photocatalyst, TiO_2 presents some disadvantages such as low exploitation of sunlight (because it is a wide gap semiconductor with values above the range 3.0-3.2 eV, and it only takes advantage of UV light) and low deNOx selectivity. Moreover, TiO_2 has just recently been proposed to be classified as possibly causing

cancer when inhaled [8]. This could limit its applications and, therefore, a rapid advance in the study and development of new deNOx photocatalysts seems reasonable.

Because of their unique properties and easy preparation, layered double hydroxides (LDHs), also known as hydrotalcite-like materials, have been studied for many potential applications in diverse and important fields such as medicine, pharmacy, catalysis, adsorption etc. [9-18]. In recent years, these compounds have also emerged as an important photocatalyst group, being widely investigated for the oxidative decomposition of aqueous contaminants and water splitting [19-21], and are promising materials in the replacement of TiO_2 [22].

LDHs are layered materials whose structure is similar to that of brucite, $Mg(OH)_2$, where a fraction of M(II) ions is replaced by M(III) ones. This generates an excess of positive charge in the layers, which are balanced by intercalating anions and water molecules in the interlayer space. The general LDH formula can be represented as $[M^{II}_{1-x} M^{III}_x(OH)_2]^{x+} X_{x/n}{}^{n-} \cdot mH_2O$, where M(II) and M(III) are divalent and trivalent cations and X is the interlayer anion. All of them may vary over a wide range and X is quite easy to exchange with other anions [23, 24]. The divalent and trivalent cations are octahedrally coordinated by hydroxide ions [25] and these edge-shared octahedral units form infinite layers with the O–H bond, perpendicular to the plane of the layers. The MO_6 octahedron is one of the key factors affecting the photocatalytic properties of LDHs, where the high dispersion of metal enables electron transfer and avoids the recombination of electrons and holes [26].

The aim of this work was to prepare several ZnAl-CO_3 layered double hydroxides with different MII/MIII ratios and to evaluate their capacity for the photodegradation of NOx as one of the more important air pollutants. However, although LDHs were studied as precursors of mixed oxides which could photocatalyze the decomposition of NOx [27], there is no report to our knowledge about pristine LDH application as photocatalysts for the oxidative decomposition process of NOx gases. Herein, the physico-chemical characterization and photocatalytic activity of different ZnAl-CO_3 LDHs are presented. Thus, by varying the synthesis procedure, it was possible to obtain LDH photocatalysts with a higher surface area and Zn content.

Moreover, the studied systems display enhanced NOx removal efficiency compared to that of benchmark TiO_2 P25, anticipating their potential use in photocatalytic building materials [28] and air purification filters [29].

2. Materials and methods.

All synthetic reagents used were at least 98–99% pure and were supplied by Sigma–Aldrich.

2.1 Preparation of LDHs

Carbonate-intercalated ZnAl-LDHs with different Zn/Al ratios were prepared by coprecipitation method at higher (named HC samples) and lower metal concentrations (named LC samples), at constant pH solutions [23, 30].

Preparation of HC samples: Solutions containing 0.2 M $Al(NO_3)_3 \cdot 9H_2O$ and 0.3, 0.4, 0.5 and 0.6 M $Zn(NO_3)_2 \cdot 6H_2O$, were slowly dropped into a suitable stochiometric concentration of NaOH and Na_2CO_3 solution, under vigorous stirring, to prepare LDHs with Zn/Al ratios of 1.5, 2, 2.5 and 3, which were named as HC1.5, HC2, HC2.5 and HC3, respectively. The suspensions thus obtained were hydrothermally treated at 80 °C and subsequently washed with distilled water, centrifuged and dried at 60 °C.

Preparation of LC samples: The same method described above was followed but the solutions were not submitted to the hydrothermal treatment. The concentrations used were of 0.03 M of $Al(NO_3)_3 \cdot 9H_2O$ and 0.045, 0.06, 0.075 and 0.09 M $Zn(NO_3)_2 \cdot 6H_2O$, and the samples were named as LC1.5, LC2, LC 2.5 and LC3, respectively.

2.2 Characterization of the photocatalysts

Powder X-ray diffraction (PXRD) patterns of powdered samples were recorded under atmospheric conditions on a Bruker D8 Discovery instrument using Cu Kα radiation (λ = 1.5405 Å) at the step size and step counting time of 0.02^{o} (2θ) and 0.65 s, respectively.

Infrared spectra were obtained on a FTIR-ATR Perkin-Elmer Spectrum Two collecting 20 scans from 450 to 4000 cm^{-1} with a resolution of 4 cm^{-1}.

The textural properties were studied by nitrogen adsorption–desorption isotherms which were recorded on a Micromeritics ASAP 2020 apparatus. Samples were previously outgassed at 100 °C under vacuum for 1 h. Specific surface areas (SSA) were calculated by applying the BET method over the relative equilibrium pressure range $0.05 < P/P_0 < 0.30$, in the N_2 adsorption isotherms. Scanning electron microscopy (SEM) images were recorded in a Helios Nanolab 650 instrument.

Mg and Al elemental chemical analyses were performed on ICP mass (Perkin Elmer Nexion X) after the dissolution of LDH in 0.1M HCl. The amount of water LDH samples was determined by thermogravimetric analysis (TGA) on a Setaram Setsys Evolution 16/18 Apparatus Leading equipment at a heating rate of 5 °C·min^{-1}.

Diffuse reflectance (DR) spectra were recorded at a scan rate of 30 nm min^{-1} from 300 to 900 nm in 0.5 nm steps, using a Varian Cary 1E spectrophotometer.

The nitrate content in the samples, after the photocatalytic test, was measured using a Perkin-Elmer model Lambda 3B UV–visible spectrophotometer. Thus, the selected sample was washed with Milli-Q water, stirred for 30 min and centrifuged. The nitrate content in the filtered solution was determined following a simple spectrophotometric method previously reported by Miranda et al. [31].

2.3 Photocatalytic activity measurement

The photochemical NO abatement test was performed by using a 50 x 50 mm sample holder placed in a laminar flow reactor. The reactor was placed inside a Solarbox 3000e RH light irradiation box equipped with an Xe lamp with controlled irradiance (Fig. S1). 500 mg of LDH sample was used in each test and irradiated with artificial sunlight (25 and 580 W m^{-2} for UV and visible). As a pollutant, a mixture of air/NO (obtained by mixing synthetic air and pure NO) was sent to the photoreactor with a NO concentration of 150 and 600 ppb. A 50 ± 5% relative humidity of the supplied gas is maintained when air is previously passed through a gas-washing bottle, filled with demineralized water. The flow rate, Q, is fixed at 0.30 L min^{-1}. The accurate measurement of the concentration of NO, NO_X and NO_2 was carried out using

a chemiluminescence analyzer (model Environment AC32M). For each test, and before the irradiation, the air/NO gas stream was passed over the sample in the dark for a period of 30 min to discard the existence of NO_X adsorption. On the other hand, NO photolysis was not observed when the test was performed in the absence of a photocatalyst. Each test was repeated three times to obtain average concentration values. The nitrogen oxide gas concentration values measured were discussed following the following parameters:

$$\text{NO conversion (\%)} = \{([NO]_{in} - [NO]_{out})/[NO]_{in}\} \times 100 \quad (1)$$

$$NO_2 \text{ released (\%)} = ([NO_2]_{out}/[NO]_{in}) \times 100 \quad (2)$$

$$NO_X \text{ conversion (\%)} = \{([NO_X]_{in} - [NO_X]_{out})/[NO_X]_{in}\} \times 100 \quad (3)$$

where $[NO]_{in}$, $[NO_X]_{in}$ and $[NO]_{out}$, $[NO_X]_{out}$ denote the measured inlet and outlet concentrations, respectively, while $[NO_X] = [NO] + [NO_2]$.

3. Results and Discussion

3.1 Characterization of the samples

PXRD patterns, included in Fig. 1, are characteristic of layered double hydroxides with a rhombohedral symmetry. The basal diffraction plane with its corresponding harmonics recorded (0 0 l) indicate the formation of layered material, and were similar to those reported by other authors for similar LDH samples [22, 25]. The basal spacings, d_{003} obtained for all ZnAl-CO_3 samples (7.6 Å) correspond to a LDH compound containing carbonate [32].

The PXRD reflection peaks of HC (hydrothermally treated) samples (Fig.1a) were sharp and narrow, showing well crystallized systems. The patterns of HC1.5 and HC2 were almost the same except for the value $d_{(110)}$ which slightly decreased for HC1.5 (from 1.53 Å to 1.52 Å) in agreement with the decrease of molar ratio Zn/ Al and the smaller size of Al^{3+} (0.675 Å) compared to Zn^{2+} ions (0.88 Å) [33]. However, as has been previously reported [34], for the initial molar ratio M(II)/M(III) greater than 2.2, it was not possible to obtain a pure LDH phase for the carbonate-intercalate ZnAl-LDH, under conditions described for HC samples. The PXRD patterns of HC 2.5 and HC 3 show

reflections at 32 and 37 2Θ degrees, assigned to the formation of an additional phase of ZnO. As reported by Vayssiers [35], this could be due to a hydrothermal temperature which can provoke condensations of Zn-OH via dehydration to form an additional ZnO phase in an aqueous media. Thus, we prepared LDH with a molar ratio Zn/Al =3 without thermal treatment. Nevertheless, an additional $Zn(OH_4)^{2-}$ phase was observed (not shown). When we prepared LDH at low metal concentrations (LC) and without thermal treatment, only a pure LDH phase was observed in PXRD patterns in the whole Zn/Al ratio range (Fig.1b) For our subsequent photocatalytic experiments, we used only pure LDH samples, i.e. HC1.5, HC2, LC1.5, LC2, LC2.5 and LC3.

Chemical analysis data are shown in Table 1 and indicate that Zn/Al molar ratios in the samples are similar to those of the starting solution used to prepare LDHs. The number of water molecules has been calculated from the first weight loss in the TG curve. These data together with Zn/Al atomic ratio have been used to propose chemical formulae of the samples, assuming that the carbonate anions compensate all positive charge of Al ions.

Table 1. Chemical and physical properties for the LDH samples: metal content and ratio; proposed formulae; BET surface and band gap energy value.

Sample	% Wt		Atomic ratio	Proposed Formulae	S_{BET}	Band gap
	Zn	Al	Zn/Al		(m^2g^{-1})	(eV)
HC 1.5	37.10	10.3	1.48	$[Zn_{0.59}Al_{0.41}(OH)_2](CO_3)_{0.20}.\ 0.44H_2O]$	32.83	3.59
HC2	40.47	8.03	2.07	$[Zn_{0.67}Al_{0.33}(OH)_2](CO_3)_{0.16}.\ 0.73H_2O]$	23.34	3.57
LC 1.5	39.09	10.50	1.53	$[Zn_{0.61}Al_{0.39}(OH)_2](CO_3)_{0.19}.\ 0.22H_2O]$	77.86	3.45
LC 2	43.20	8.43	2.12	$[Zn_{0.66}Al_{0.31}(OH)_2](CO_3)_{0.16}.\ 0.24H_2O]$	44.75	3.56
LC 2.5	43.28	7.00	2.55	$[Zn_{0.72}Al_{0.28}(OH)_2](CO_3)_{0.14}.\ 0.17H_2O]$	52.11	3.41
LC 3	45.96	6.40	3.05	$[Zn_{0.76}Al_{0.24}(OH)_2](CO_3)_{0.12}.\ 0.10H_2O]$	56.16	3.53

The FT-IR spectra of the original LDH samples (Supplementary Fig. S2) were all similar and presented bands of around 3500 cm^{-1} corresponding to the hydroxyl stretching vibration mode, both from the layer groups and from the water molecules. A small shoulder at 1630 cm^{-1} corresponds to the bending mode of the interlayer water, a rather strong band at 1380 cm^{-1} due to the vibration mode v3 of the interlayer carbonate anion, and the bands below 900 $^{-1}$ are due to the M-O vibration and M-O-H bending modes.

As observed from SEM images (Fig.2), the LDH nanocrystals showed a hexagonal sheet-like morphology in accordance with the layered structure confirmed by PXRD technique. HC samples exhibited well defined hexagonal layer crystals with width and height dimensions of less than 470 and 60 nm, respectively. On the other hand, a poorer crystallization was observed for LC samples, whose crystal dimensions were less than 380 and 40 nm, respectively. In both types of synthesis, HC and LC, the nanocrystals became larger as the Zn/Al ratio increased.

Adsorption-desorption isotherms of N_2 have been carried out to study the textural properties of the samples, and some selected examples are shown in Fig. 3. According to IUPAC classification [36], the isotherms correspond to a type II with a contribution of type IV, and were similar to those reported for LDH compounds [22, 37]. Type II is assigned to the adsorption on macro and non-porous materials, although hysteresis loops also suggest the presence of mesopores. Since the N_2 diameter is larger than the interlamellar space for carbonate containing layered double hydroxides, the specific surface areas correspond to the external surface, and the pore volume to interparticle pores. The H3 loop is characteristic of non-restricted multilayer adsorption at high relative pressures, and it is observed in aggregates of plate-like particles giving rise to slit-like pores [36]. Specific surface areas determined by BET method are given in Table 1 and were higher for LC samples, which is in agreement with their lower cristallinity (due to the fact that these samples were not submitted to hydrothermal treatment), as was confirmed by PXRD (Fig. 1) and SEM characterization (Fig. 2).

Additional characterisation concerning the light activation of the samples was performed. The light absorption, which corresponds to electron excitation from the valence band to the conduction band, can be used to determine the nature and value of the optical band gap (E_g). The acquired diffused reflectance spectra were converted to the Kubelka–Munk function $[F(R_\infty)h\nu]^2$. The band gap energies of the samples are estimated from the tangent lines in the plots of the modified Kubelka–Munk function vs. the energy of exciting light [38] (Fig. 4). The estimated band-gap values ranging between 3.41 and 3.59 eV are in line with those reported for pure ZnAl LDHs (Table 1), which are UV light responsive [39-41].

3.2 deNO_X photocatalytic tests

The photochemical ability of LDH samples to abate the concentration of NO polluted atmospheres was studied. The photocatalytic removal of NO gas in air is thought to occur through its complete oxidation to nitrate species. This photochemical oxidation (PCO) process is complex and involves several steps and intermediate species [42, 43]. The deNOx PCO mechanism proposed is the same as that proposed for semiconductors such as TiO_2, Fe_2O_3 and ZnO [43-45]:

$$Zn/Al–LDH + h\nu \rightarrow Zn/Al–LDH^* (h_{vb}^+ + e_{cb}^-) \quad (4)$$

$$h_{vb}^+ + H_2O \rightarrow \cdot OH + H^+ \quad (5)$$

$$e_{cb}^- + O_2 \rightarrow \cdot O_2^- \quad (6)$$

$$\cdot O_2^- + H^+ \rightarrow \cdot OOH \quad (7)$$

$$NO + 2\cdot OH \rightarrow NO_2 + H_2O \quad (8)$$

$$NO_2 + \cdot OH \rightarrow NO_3^- + H^+ \quad (9)$$

$$NO_X + \cdot O_2^- \rightarrow NO_3^- \quad (10)$$

Once a Zn/Al–LDH molecule adsorbs a UV light photon with energy equal or greater than its band gap (≈ 3.5 eV), the excited electron of LDH is transferred from the valence band (VB) to the conduction band (CB), and pairs of mobile charges (e- and h+) reach the surface of the semiconductor particles [41, 46]. Now, in the presence of adsorbed water molecules, reactive oxygen species (ROS) are formed (reactions 5 to 7), initiating the progressive oxidation of NO gas (reactions 8 to 10).

Figure 5a shows the concentration profiles of the evolution of nitrogen oxide gases recorded for the HC2 sample as a function of light irradiation time, as an example. In the dark for the first 30 min, the inlet NO concentration was constant. Therefore, the possibility of NO gas adsorption on the LDH particle surface was discarded. Conversely, under irradiation, the NO concentration decreased suddenly indicating that light exposure was essential to trigger the process. The NO removal rapidly increased on time (60 min) and then approached an almost constant value, indicating the achievement of a stable photo-oxidation activity. The photochemical process stopped when illumination was shut down.

The decrease in NO concentration values measured under light condition is related to the amount of removed NO. Thus, following the NO conversion profiles in Figure 5b, a clear dependence between photocatalytic efficiency and surface area values was observed, as expected. NO removal efficiencies around 55 % were found for LC samples, exhibiting almost double the surface area in comparison to that of HC samples, whose NO removal efficiencies were limited to 33 %. Nevertheless, the Zn/Al ratio must also be taken into account in order to explain some differences observed between the NO conversion profiles. Thus, during the first ten minutes of irradiation, the NO conversion increases more quickly in samples with a higher Zn/Al ratio. As expected, as the amount of Zn active centres increase on the catalyst, the kinetic of the PCO process is enhanced. However, when a steady state is reached, at around thirty minutes of irradiation, the difference in the amount of Zn in the samples does not seem to clearly alter the photochemical performance. Therefore, the Zn/Al-LDH samples show high efficiency for NO conversion in the whole 1.5 to 3.0 metal ratio range, the surface area being a characteristic of greater importance. As described before, by changing the method of preparation from HC to LC, the samples develop high surface area values and, therefore, exhibit the best photochemical efficiency. It is of high importance to pay attention to the release of NO_2 accounted for during the irradiation period (Fig. 5a), as a product of reaction (6). The appearance of nitrogen dioxide as an intermediate specie is undesired as it is much more dangerous than NO [47]. In this sense, the optimization of a $deNO_X$ photocatalyst is focused on obtaining the highest NO conversion values but also to restrict the NO_2 emissions. Therefore, it is of interest to know about the photocatalyst deNOx selectivity [48], *S*, which is determined according to the equation:

$$S\,(\%) = \frac{([\mathrm{NOx}]_{\mathrm{in}} - [\mathrm{NOx}]_{\mathrm{out}})/[\mathrm{NOx}]_{\mathrm{in}}}{([\mathrm{NO}]_{\mathrm{in}} - [\mathrm{NO}]_{\mathrm{out}})/[\mathrm{NO}]_{\mathrm{in}}} \times 100 \qquad (11)$$

indicating the ratio of degraded NO that is ultimately converted into harmless nitrate (reactions 8 to 10), rather than into toxic nitrogen dioxide. Fig. 5c shows the NO and NO_X conversion, the NO_2 release and the *S* values measured from $deNO_X$ tests performed on HC and LC phototacalysts. For comparison, S values for Aeroxide® TiO_2 P25 (Evonik) – a material broadly used worldwide as a reference in photocatalytic

deNO$_X$ processes – were also obtained. TiO_2 P25 exhibits similar physical characteristics to LC samples, with nanoparticles around 20-50 nm in size, and with a surface area of 52.4 $m^2 g^{-1}$.

The LC samples not only exhibit the highest NO conversion values, but also the lowest NO_2 emissions (around 6 %), reaching a NOx gas removal value of 50 %. Therefore, the selectivity of these systems is surprisingly high with S values of around 90%. To our knowledge, these values are scarcely reported and only for some TiO_2 advanced photocatalysts [5, 49-52]. In fact, when compared to a TiO_2 P25 benchmark product, even though a somewhat higher photocatalytic performance for the NO oxidation (63%) is observed, the NOx removal is limited to 42 % because the selectivity falls to 42%. The low deNOx selectivity of titania oxides is due to the continuously increased emission of NO_2 under light irradiation [53], as observed in the test shown in Fig. S3. On the other hand, in agreement with our findings, low NO_2 release is also found in ZnO deNO$_X$ photocatalysts [54] being associated with the sensitivity of this oxide to NO_2 gas [55]. Also, when compared with commercial ZnO nanopowders (< 100 nm; Aldrich 544906), the LDHs exhibit better photocatalytic efficiency (Figures 5c and S2).

Additional experiments were performed in order to qualitatively characterize the potential application of these photocatalysts. Firstly, the photocatalyst reusability was preliminarily investigated for LC1.5 and LC3 samples. Three consecutive NO photocatalytic removal experiments were run in periods of 60 min. Between experiments, the samples were washed with water, centrifuged, collected and dried to eliminate nitrate species. The data collected (Fig. 6a) so far, suggest that no significant changes in the photocatalytic efficiency took place. Moreover, the high deNOx selectivity remained constant as the NO_2 emission was low and constant during the three runs. The excellent photocatalyst reusability found is in line with the fact that no chemical or structural changes were observed after photocatalysis and that surface area values is recovered after washing process (Fig. S4, S5 and S6). On the other hand, we evaluate the potential ability of these photocatalysts to confront to NO urban pollution, in a qualitative way. Fig. 6b shows the diurnal mean values of NO concentration measured at urban roadsides in a highly populated city [56]. During daylight hours, the NO concentration increased rapidly after sunrise and reached its maximum level

between 7-12 in the morning. In this sense, we have proved the activity of the LC3 sample in an extended period of five hours under similar NO concentrations. Thus, initiating a De-NOx test with 150 ppb, the LC3 sample once again showed high and constant NO conversion values around 50% during this extended light irradiation period. Moreover, the selectivity (data not shown) was maintained around 90 %. This extended experiment was also useful in confirming the formation and deposition of nitrate onto the surface of the LDH samples, as expected from the PCO mechanism proposed. To consider the nitrogen mass balance during the photocatalytic oxidation process on the sample, taking into account the concentration of NO in the inlet gas and the gas flow rate, the integral area of the NOx plot gives the amount of NO transformed into NO_3^- during the irradiation time [52], from which, 28.10 μg of nitrate was calculated to be formulated on the photocatalyst. This value is close to that chemically analysed in the corresponding washing solution obtained from LC3 samples, 27.8 μg. On the other hand, the good De-NOx performance of LC3 was also observed in an atmosphere with a higher NO concentration. Thus, similar efficiencies were found when samples were used under NO 600 ppb inlet concentration, Fig. S.7. The new findings from this research serve to anticipate the potential of ZnAl-CO_3 LDH photocatalysts in real life applications. Thus, when added to materials exposed to urban atmosphere (e.g. building materials, paints, metal covering …) it confers the ability to abate most of the NO concentration present in the environment. As we have demonstrated the easiness of washing and the reusability of the photocatalyst, this action is permanent as the surface of materials is continuously cleaned by the dew and rain water. Moreover, because of their capacity to abate high NO concentrations, the use of ZnAl-CO_3 LDH photocatalysts could be envisaged for other deNOx applications, [57] for example, in air cleaning devices. From these qualitative data, the NO urban pollution could potentially be greatly minimized with the use of ZnAl LDH photocatalysts.

4. Conclusions

LDH photocatalysts were found to be active for the photochemical oxidation of NO gas for the first time. ZnAl-CO_3 LDHs were prepared by the coprecipitation method at high (HC samples) and low metal concentrations (LC samples). Pure LDH phase is obtained in LC samples for Zn/Al ratio as high as 3.0. However, in the case of HC samples, an additional ZnO phase was found for Zn/Al ratio superior to 2.0. For all the prepared LDH samples, the IR spectra indicated the presence of interlayer carbonate anions. The synthetic procedure affected the crystalline growth. Well defined and larger hexagonal nanolayers were found in HC samples, while the LC samples were smaller and with poorer crystallization. The largest crystals were found when the Zn/Al ratio was increased,

While the pore microstructure was similar for HC and LC samples. Because of the lower crystallinity of LC samples, the estimated specific surface area values (around 55 $m^2 \cdot g^{-1}$) were almost double that of the HC samples. The ZnAl-CO_3 LDHs were UV light responsive with band–gap values close to 3.5 eV. High NO removal efficiencies around 55 % were found. The photocatalytic efficiency was related to the surface area of the samples, being higher in the case of LC samples. In comparison with the TiO_2 P25 benchmark product, ZnAl-CO_3 LDHs exhibited impressive selectivity to the deNOx process. Moreover, the studied photocatalysts maintain the same NO removal efficiency and selectivity for an extended period and in the highest NO concentration experiments. The easy and inexpensive preparation of the ZnAl-CO_3 LDHs and the promising deNOx results obtained here, open new and interesting perspectives for their potential use in urban air remediation.

Acknowledgements

This work was partly financed by the Junta de Andalucía (PAI Groups FQM-214 and FQM-175) and Spanish Government (MAT2017-88284-P). Rodriguez-Rivas acknowledges a grant from the Fundación Carolina to research at the University of Córdoba (Spain).

References

[1] European Environment Agency.
[2] J.A. Last, W.M. Sun, H. Witschi, Ozone, NO, and NO_2: oxidant air pollutants and more, Environ. Health Perspect. 102 (1994) 179-184.
[3] B. Chen, C. Hong, H. Kan, Exposures and health outcomes from outdoor air pollutants in China, Toxicology 198 (2004) 291-300.
[4] S.A. Cormier, S. Lomnicki, W. Backes, B. Dellinger, Origin and Health Impacts of Emissions of Toxic By-Products and Fine Particles from Combustion and Thermal Treatment of Hazardous Wastes and Materials, Environ. Health Perspect. 114 (2006) 810-817.
[5] T. Giannakopoulou, I. Papailias, N. Todorova, N. Boukos, Y. Liu, J. Yu, C. Trapalis, Tailoring the energy band gap and edges' potentials of g-C_3N_4/TiO_2 composite photocatalysts for NOx removal, Chem. Eng. J. 310 (2017) 571-580.
[6] B. Tan, X. Zhang, Y. Li, H. Chen, X. Ye, Y. Wang, J. Ye, Anatase TiO_2 Mesocrystals: Green Synthesis, In Situ Conversion to Porous Single Crystals, and Self-Doping Ti^{3+} for Enhanced Visible Light Driven Photocatalytic Removal of NO, Chem. Eur. J. 23 (2017) 5478-5487.
[7] S. Karapati, T. Giannakopoulou, N. Todorova, N. Boukos, I. Papailias, D. Dimotikali, C. Trapalis, Novel 'Pickering' modified TiO_2 photocatalysts with high De-NOx efficiency, Catal. Today 287 (2017) 45-51.
[8] European Chemical Agency, ANNEX 2 - Comments and response to comments on CLH proposal on titanium dioxide 2017.
[9] V. Ambrogi, G. Fardella, G. Grandolini, L. Perioli, Intercalation compounds of hydrotalcite-like anionic clays with antiinflammatory agents — I. Intercalation and in vitro release of ibuprofen, Int. J. Pharm. 220 (2001) 23-32.
[10] J.-H. Choy, S.-Y. Kwak, J.-S. Park, Y.-J. Jeong, Cellular uptake behavior of [[gamma]-32P] labeled ATP-LDH nanohybrids, J. Mater. Chem. 11 (2001) 1671-1674.
[11] D.G. Evans, X. Duan, Preparation of layered double hydroxides and their applications as additives in polymers, as precursors to magnetic materials and in biology and medicine, Chem. Commun. (Cambridge, U. K.) (2006) 485-496.
[12] F. Bruna, I. Pavlovic, R. Celis, C. Barriga, J. Cornejo, M.A. Ulibarri, Organohydrotalcites as novel supports for the slow release of the herbicide terbuthylazine, Appl. Clay Sci. 42 (2008) 194-200.
[13] M.A. González, I. Pavlovic, C. Barriga, Cu(II), Pb(II) and Cd(II) sorption on different layered double hydroxides. A kinetic and thermodynamic study and competing factors, Chem. Eng. J. 269 (2015) 221-228.
[14] K. Abdellaoui, I. Pavlovic, M. Bouhent, A. Benhamou, C. Barriga, A comparative study of the amaranth azo dye adsorption/desorption from aqueous solutions by layered double hydroxides, Appl. Clay Sci. 143 (2017) 142-150.
[15] X. Xiang, L. Xie, Z. Li, F. Li, Ternary MgO/ZnO/In2O3 heterostructured photocatalysts derived from a layered precursor and visible-light-induced photocatalytic activity, Chem. Eng. J. 221 (2013) 222-229.
[16] Y. Tang, R. Wang, Y. Yang, D. Yan, X. Xiang, Highly Enhanced Photoelectrochemical Water Oxidation Efficiency Based on Triadic Quantum Dot/Layered Double Hydroxide/BiVO4 Photoanodes, ACS Appl. Mater. Interfaces 8 (2016) 19446-19455.
[17] W. He, R. Wang, L. Zhang, J. Zhu, X. Xiang, F. Li, Enhanced photoelectrochemical water oxidation on a BiVO4 photoanode modified with multi-functional layered double hydroxide nanowalls, J. Mater. Chem. A 3 (2015) 17977-17982.
[18] Y. Li, L. Zhang, X. Xiang, D. Yan, F. Li, Engineering of ZnCo-layered double hydroxide nanowalls toward high-efficiency electrochemical water oxidation, J. Mater. Chem. A 2 (2014) 13250-13258.

[19] G. Fan, F. Li, D.G. Evans, X. Duan, Catalytic applications of layered double hydroxides: recent advances and perspectives, Chem. Soc. Rev. 43 (2014) 7040-7066.
[20] X. Xiang, F. Li, Z. Huang, Recent Advances in Layered Double Hydroxide-Based Materials as Versatile Photocatalysts, Rev. Adv. Sci. Eng. 3 (2014) 158-171.
[21] L. Mohapatra, K. Parida, A review on the recent progress, challenges and perspective of layered double hydroxides as promising photocatalysts, J. Mater. Chem. A 4 (2016) 10744-10766.
[22] D. Carriazo, M. del Arco, E. García-López, G. Marcì, C. Martín, L. Palmisano, V. Rives, Zn,Al hydrotalcites calcined at different temperatures: Preparation, characterization and photocatalytic activity in gas–solid regime, J. Mol. Catal. A: Chem. 342-343 (2011) 83-90.
[23] W.T. Reichle, Synthesis of anionic clay minerals (mixed metal hydroxides, hydrotalcite), Solid State Ionics 22 (1986) 135-141.
[24] P. Braterman, Z. Ping Xu, F. Yarberry, Layered Double Hydroxides (Ldhs), 2005.
[25] F. Cavani, F. Trifirò, A. Vaccari, Hydrotalcite-type anionic clays: Preparation, properties and applications, Catal. Today 11 (1991) 173-301.
[26] X.D. Wang, C.J. Summers, Z.L. Wang, Mesoporous Single-Crystal ZnO Nanowires Epitaxially Sheathed with Zn_2SiO_4, Adv. Mater. 16 (2004) 1215-1218.
[27] M. Sarkarat, S. Komarneni, Z. Rezvani, X. Wu, S. Yin, TsugioSato, Z.-F. Yan, Multi-cationic layered double hydroxides: Calcined products as photocatalysts for decomposition of NOx, Appl. Clay Sci. 80-81 (2013) 390-397.
[28] A. Folli, C. Pade, T.B. Hansen, T. De Marco, D.E. Macphee, TiO_2 photocatalysis in cementitious systems: Insights into self-cleaning and depollution chemistry, Cem. Concr. Res. 42 (2012) 539-548.
[29] C.H. Ao, S.C. Lee, Indoor air purification by photocatalyst TiO2 immobilized on an activated carbon filter installed in an air cleaner, Chem. Eng. Sci. 60 (2005) 103-109.
[30] E.M. Seftel, E. Popovici, M. Mertens, K.D. Witte, G.V. Tendeloo, P. Cool, E.F. Vansant, Zn–Al layered double hydroxides: Synthesis, characterization and photocatalytic application, Microporous Mesoporous Mater. 113 (2008) 296-304.
[31] K.M. Miranda, M.G. Espey, D.A. Wink, A Rapid, Simple Spectrophotometric Method for Simultaneous Detection of Nitrate and Nitrite, Nitric Oxide 5 (2001) 62-71.
[32] I. Crespo, C. Barriga, V. Rives, M.A. Ulibarri, Intercalation of iron hexacyano complexes in Zn,Al-hydrotalcite, Solid State Ionics 101-103 (1997) 729-735.
[33] J.E. Huheey, E.A. Keiter, R.L. Keiter, O.K. Medhi, Inorganic Chemistry: Principles of Structure and Reactivity, Pearson Education2006.
[34] V. Rives, Layered double hydroxides: present and future, Nova Publishers2001.
[35] L. Vayssieres, Growth of arrayed nanorods and nanowires of ZnO from aqueous solutions, Adv. Mater. 15 (2003) 464-466.
[36] K.S. Sing, Reporting physisorption data for gas/solid systems with special reference to the determination of surface area and porosity (Recommendations 1984), Pure Appl. Chem. 57 (1985) 603-619.
[37] R. Extremera, I. Pavlovic, M.R. Pérez, C. Barriga, Removal of acid orange 10 by calcined Mg/Al layered double hydroxides from water and recovery of the adsorbed dye, Chem. Eng. J. 213 (2012) 392-400.
[38] A.A.A. Ahmed, Z.A. Talib, M.Z. bin Hussein, A. Zakaria, Zn–Al layered double hydroxide prepared at different molar ratios: Preparation, characterization, optical and dielectric properties, J. Solid State Chem. 191 (2012) 271-278.
[39] G. Starukh, Photocatalytically Enhanced Cationic Dye Removal with Zn-Al Layered Double Hydroxides, Nanoscale Res Lett 12 (2017) 391.
[40] S. Babakhani, Z.A. Talib, M.Z. Hussein, A.A.A. Ahmed, Optical and thermal properties of Zn/Al-layered double hydroxide nanocomposite intercalated with sodium dodecyl sulfate, J. Spectrosc. 2014 (2014).

[41] S.-M. Xu, T. Pan, Y.-B. Dou, H. Yan, S.-T. Zhang, F.-Y. Ning, W.-Y. Shi, M. Wei, Theoretical and experimental study on MIIMIII-layered double hydroxides as efficient photocatalysts toward oxygen evolution from water, J. Phys. Chem. C 119 (2015) 18823-18834.
[42] S. Devahasdin, C. Fan, K. Li, D.H. Chen, TiO_2 photocatalytic oxidation of nitric oxide: transient behavior and reaction kinetics, J. Photochem. Photobiol. A 156 (2003) 161-170.
[43] J. Balbuena, M. Cruz-Yusta, L. Sánchez, Nanomaterials to Combat NO_X Pollution, J. Nanosci. Nanotechnol. 15 (2015) 6373-6385.
[44] R. Sugrañez, J. Balbuena, M. Cruz-Yusta, F. Martín, J. Morales, L. Sánchez, Efficient behaviour of hematite towards the photocatalytic degradation of NO_X gases, Appl. Catal. B: Environ. 165 (2015) 529-536.
[45] Y. Wei, Y. Huang, J. Wu, M. Wang, C. Guo, D. Qiang, S. Yin, T. Sato, Synthesis of hierarchically structured ZnO spheres by facile methods and their photocatalytic deNOx properties, J. Hazard. Mater. 248-249 (2013) 202-210.
[46] S.-J. Xia, F.-X. Liu, Z.-M. Ni, J.-L. Xue, P.-P. Qian, Layered double hydroxides as efficient photocatalysts for visible-light degradation of Rhodamine B, J. Colloid Interface Sci. 405 (2013) 195-200.
[47] R.J. Lewis, N.I. Sax, Sax's Dangerous Properties of Industrial Materials, 12th ed., Van Nostrand Reinhold, New York, 2012.
[48] J.Z. Bloh, A. Folli, D.E. Macphee, Photocatalytic NO_X abatement: why the selectivity matters, RSC Adv. 4 (2014) 45726-45734.
[49] J. Ma, H. Wu, Y. Liu, H. He, Photocatalytic Removal of NO_X over Visible Light Responsive Oxygen-Deficient TiO_2, J. Phys. Chem. C 118 (2014) 7434-7441.
[50] N. Todorova, T. Giannakopoulou, S. Karapati, D. Petridis, T. Vaimakis, C. Trapalis, Composite TiO_2/clays materials for photocatalytic NO_X oxidation, Appl. Surf. Sci. 319 (2014) 113-120.
[51] A. Trapalis, N. Todorova, T. Giannakopoulou, N. Boukos, T. Speliotis, D. Dimotikali, J. Yu, TiO_2/graphene composite photocatalysts for NO_X removal: A comparison of surfactant-stabilized graphene and reduced graphene oxide, Appl. Catal. B: Environ. 180 (2016) 637-647.
[52] A.V. Katsanaki, A.G. Kontos, T. Maggos, M. Pelaez, V. Likodimos, E.A. Pavlatou, D.D. Dionysiou, P. Falaras, Photocatalytic oxidation of nitrogen oxides on N-F-doped titania thin films, Appl. Catal. B: Environ. 140–141 (2013) 619-625.
[53] M.J. Hernández Rodríguez, E. Pulido Melián, O. González Díaz, J. Araña, M. Macías, A. González Orive, J.M. Doña Rodríguez, Comparison of supported TiO_2 catalysts in the photocatalytic degradation of NO_X, J. Mol. Catal. A: Chem. 413 (2016) 56-66.
[54] N. Todorova, T. Giannakopoulou, K. Pomoni, J. Yu, T. Vaimakis, C. Trapalis, Photocatalytic NOx oxidation over modified ZnO/TiO_2 thin films, Catal. Today 252 (2015) 41-46.
[55] S. Öztürk, N. Kılınç, N. Taşaltin, Z.Z. Öztürk, A comparative study on the NO_2 gas sensing properties of ZnO thin films, nanowires and nanorods, Thin Solid Films 520 (2011) 932-938.
[56] S.K. Pandey, K.-H. Kim, S.-Y. Chung, S.J. Cho, M.Y. Kim, Z.-H. Shon, Long-term study of NO_X behavior at urban roadside and background locations in Seoul, Korea, Atmos. Environ. 42 (2008) 607-622.
[57] A. Šuligoj, U.L. Štangar, A. Ristić, M. Mazaj, D. Verhovšek, N.N. Tušar, TiO2–SiO2 films from organic-free colloidal TiO2 anatase nanoparticles as photocatalyst for removal of volatile organic compounds from indoor air, Appl. Catal. B: Environ. 184 (2016) 119-131.

Figure captions

Figure 1: PXRD patterns of HC and LC samples (* ZnO)

Figure 2: SEM images of HC and LC samples

Figure 3: N_2 adsorption-desorption isotherms for HC and LC samples

Figure 4: Kubelka-Munk transformed reflectance spectra for HC and LC samples

Figure 5: (a) Nitrogen oxides concentration profiles obtained during the photo-degradation of gaseous NO under light irradiation on sample HC2. De-NOx performances for ZnAl-CO_3 photocatalysts: (b) NO conversion efficiencies; (c) NO and NO_X conversion, NO_2 released and selectivity values.

Figure 6: (a) NO and NO_2 concentration profiles obtained for LC1.5 (o) and LC3 (□) samples during successive experiments of photochemical degradation of NO gas under light irradiation. (b) Diurnal distribution pattern of NO gas at urban roadside (orange shading) and NO concentration profile obtained for LC3 sample (o) during 5 hours of light irradiation

Figure S1: Schematic presentation of the continuous flow gas environmental reactor used for this study. 1: MFC (Mass Flow Controllers); 2: Sample Line; 3: By-Pass Line; 4: Reaction Chamber; 5: Sample holder; 6: UV-Vis Lamps; 7: NOx Analizer; 8: Data Recorder.

Figure S2: FT-IR spectra obtained for LC samples

Figure S3: Nitrogen oxides concentration profiles obtained during the photo-degradation of gaseous NO under light irradiation on TiO_2 P25 and ZnO photocatalysts.

Figure S4: PXRD patterns of LC samples before and after the photocatalytic process

Figure S5: FT-IR spectra of LC samples before and after the photocatalytic process

Figure S6: N_2 adsorption-desorption isotherms for LC 2.5 sample before and after the photocatalytic process and after washing

Figure S7: Nitrogen oxides concentration profiles obtained during the photo-degradation of gaseous NO (600 ppb inlet concentration) under light irradiation on sample LC3.

Figure 1

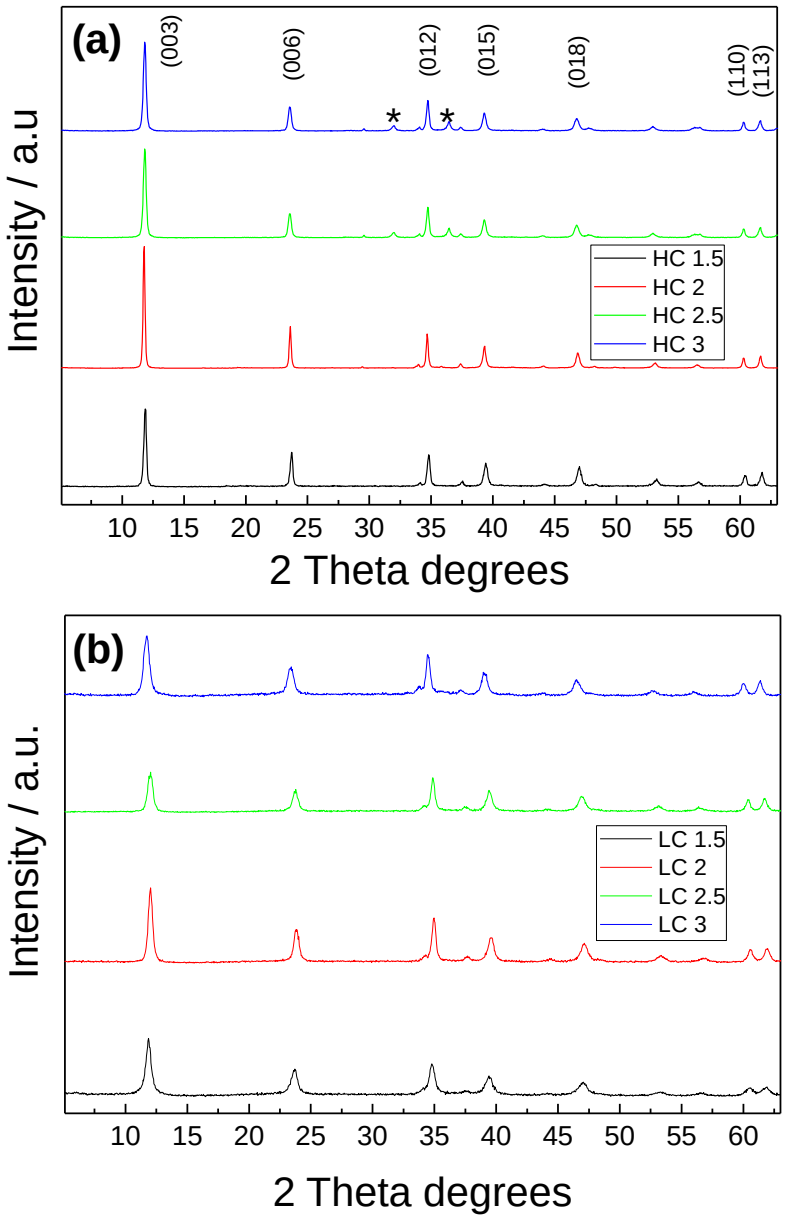

Fig 1.

Figure 2

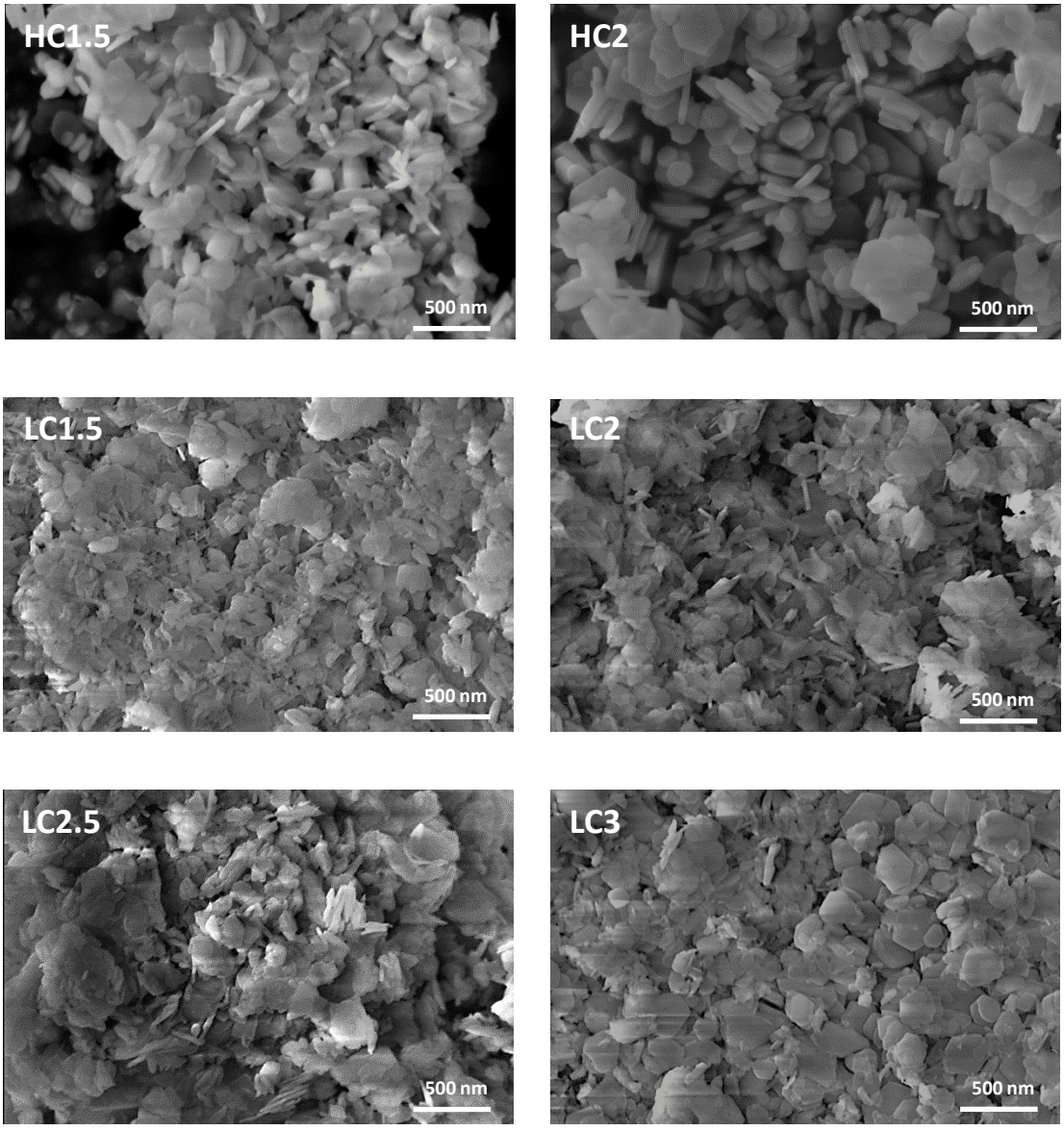

Fig 2

Figure 3

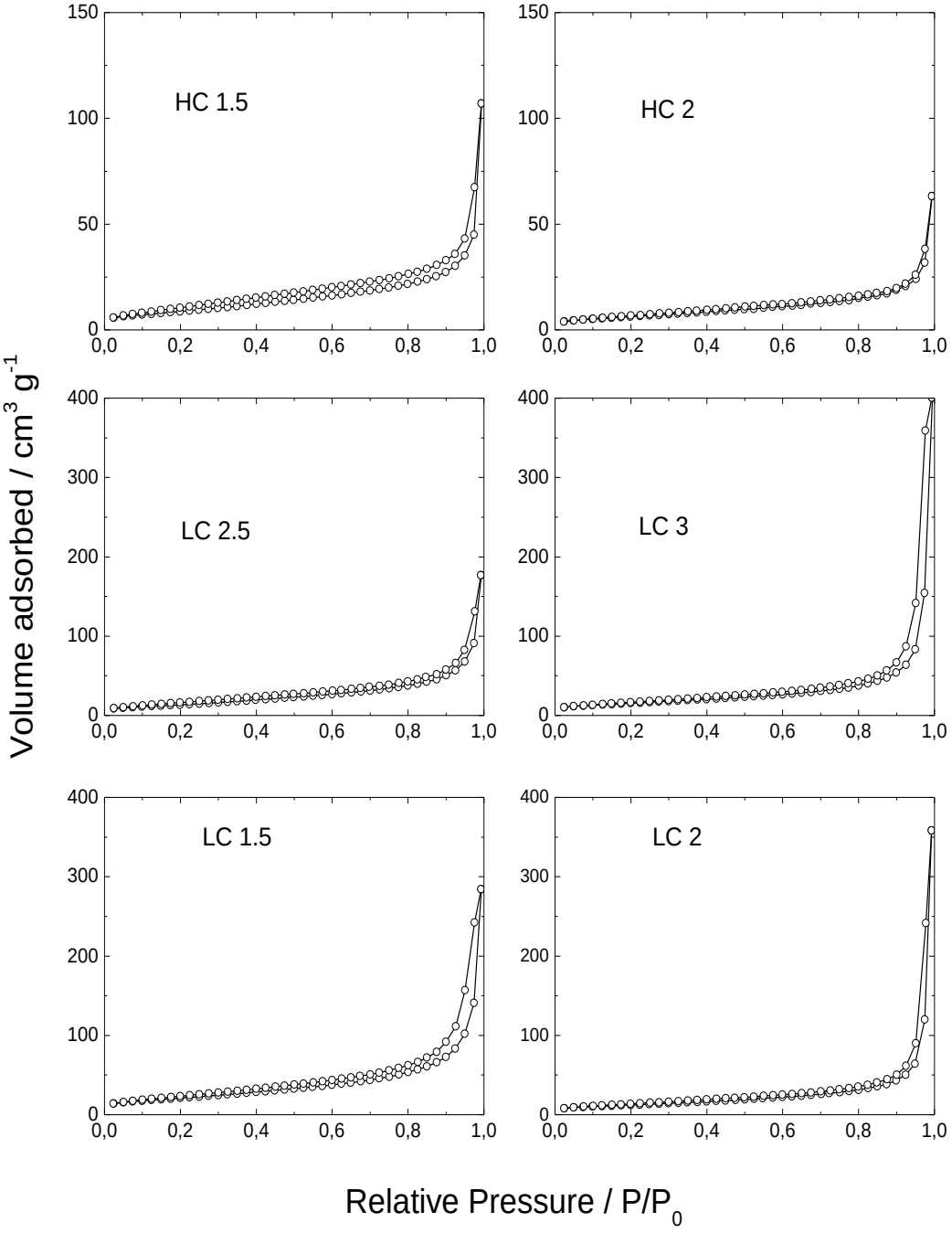

Fig. 3

Figure 4

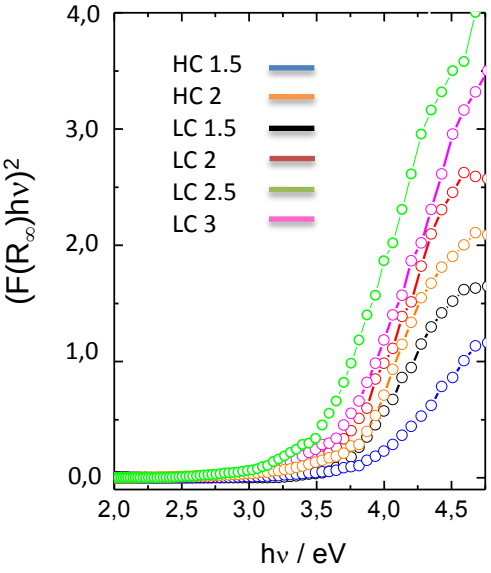

Fig. 4

Figure 5

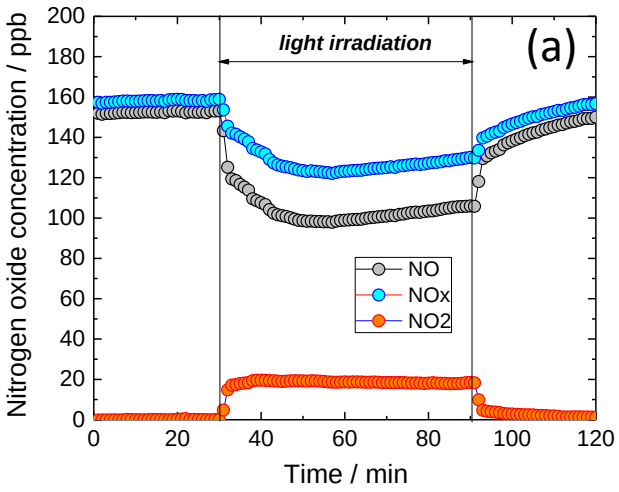

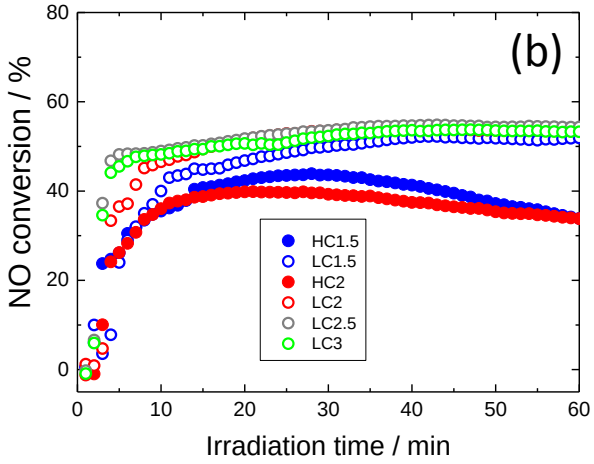

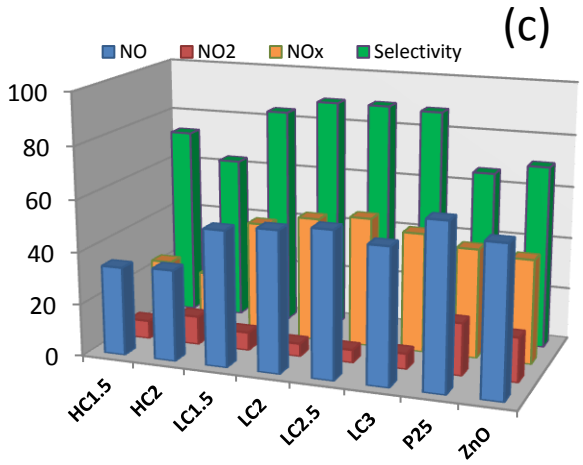

Fig 5

Figure 6

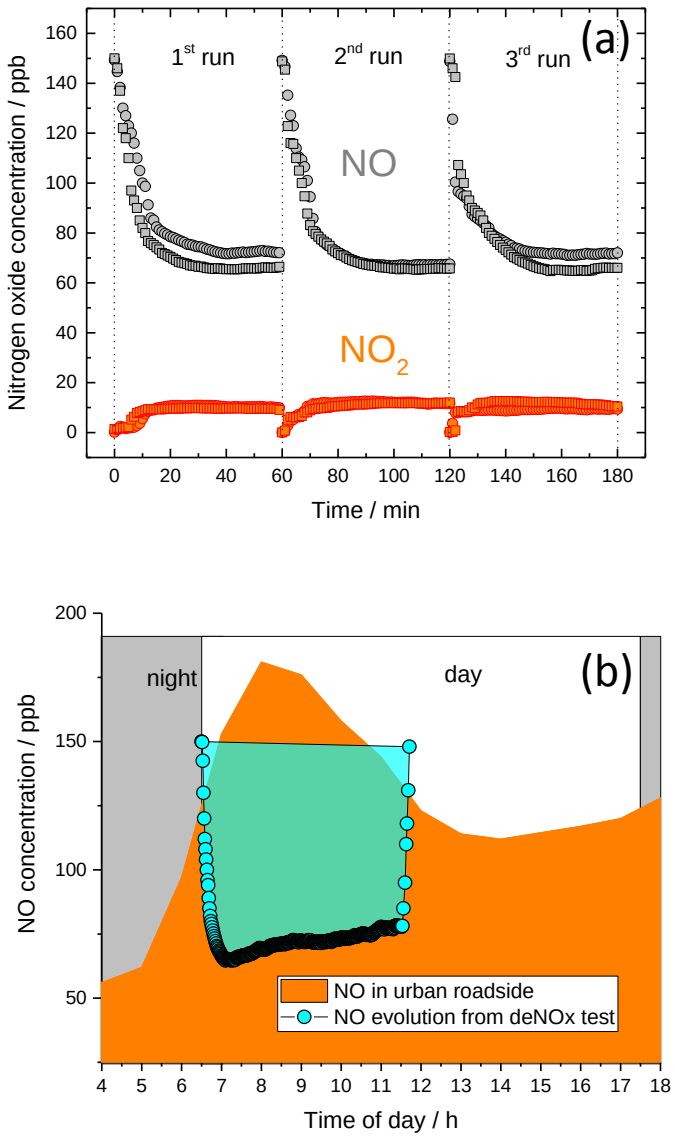

Fig 6: